JCB Journal of Cell Biology

ARTICLE

Terminal web and vesicle trafficking proteins mediate nematode single-cell tubulogenesis

Zhe Yang[1], Brendan C. Mattingly[2], David H. Hall[3], Brian D. Ackley[1], and Matthew Buechner[1]

Single-celled tubules represent a complicated structure that forms during development, requiring extension of a narrow cytoplasm surrounding a lumen exerting osmotic pressure that can burst the luminal membrane. Genetic studies on the excretory canal cell of *Caenorhabditis elegans* have revealed many proteins that regulate the cytoskeleton, vesicular transport, and physiology of the narrow canals. Here, we show that β_H-spectrin regulates the placement of intermediate filament proteins forming a terminal web around the lumen, and that the terminal web in turn retains a highly conserved protein (EXC-9/CRIP1) that regulates apical endosomal trafficking. EXC-1/IRG, the binding partner of EXC-9, is also localized to the apical membrane and affects apical actin placement and RAB-8–mediated vesicular transport. The results suggest that an intermediate filament protein acts in a novel pathway to direct the traffic of vesicles to locations of lengthening apical surface during single-celled tubule development.

Introduction

The interactions of cell cytoskeleton with vesicle trafficking are crucial to provide cells with the shape needed to perform specialized functions. For example, the microtubule and actin filament structure mediates transport of cargo to form and maintain the nerve terminal at the end of an axon (Hakanen et al., 2019; Kiral et al., 2018), Rab proteins regulate the apical specialized functions of multiple cell types in intestinal villi (Zhang and Gao, 2016), and defects affecting endosomal trafficking (in neurons and glia) underlie several neural diseases such as Charcot-Marie-Tooth disease and Niemann-Pick disease (Neefjes and van der Kant, 2014). Advances in understanding these interactions have arisen from studies in a wide range of tissues and organisms, from yeast (Chiou et al., 2017; Pires and Boxem, 2018) to *Caenorhabditis elegans* (Sato et al., 2014), *Drosophila* (Mack and Georgiou, 2014; Nemetschke and Knust, 2016), and mammalian cells such as MDCK cells in culture (Román-Fernández et al., 2018). An interesting specialized case is the formation and extension of narrow tubular structures, which require both the cytoskeletal extension to reach out to target tissues and the curvature of the apical surface to create a patent tubule (Barry et al., 2015; Sigurbjörnsdóttir et al., 2014; Sundaram and Cohen, 2017).

The excretory canal cell of *C. elegans* offers a tractable genetic model for studying single-celled tubular morphogenesis in a "seamless cell" without intracellular junctions to hold the tube together along its length (Fig. 1 a; Sundaram and Buechner, 2016; Sundaram and Cohen, 2017) This cell sends out long hollow projections that reach the length of the animal to collect and eliminate excess liquid (Falin et al., 2009; Igual Gil et al., 2017; Nelson et al., 1983; Sundaram and Buechner, 2016). While the excretory system as a whole is required for organismal survival, a large number of viable mutants have been found that impair the ability of the excretory canals to form narrow tubular extensions (Al-Hashimi et al., 2019; Buechner et al., 1999; Igual Gil et al., 2017); cloning of the underlying genes has revealed a wide variety of cytoskeletal proteins involved, including ezrin-radixin-moesin (ERM) and β_H-spectrin anchors of the actin cytoskeleton (Khan et al., 2013; Praitis et al., 2005), a diaphanous-related formin that links actin to the microtubule cytoskeleton (Shaye and Greenwald, 2015), and three intermediate filament proteins that wrap around the apical (luminal) surface to form a terminal web similar to that surrounding intestinal tubes (Al-Hashimi et al., 2018; Geisler et al., 2020; Karabinos, 2019; Khan et al., 2019; Kolotuev et al., 2013).

In addition, vesicle trafficking is important for canal morphogenesis. Mutants impairing function of the exocyst (Armenti et al., 2014) show profound defects in canal formation, as do mutations affecting the CCM-3/STRIPAK machinery that maintain normal mammalian brain capillary morphology (Lant et al., 2015). Finally, three proteins affecting vesicle transport

[1]Department of Molecular Biosciences, University of Kansas, Lawrence, KS; [2]Department of Undergraduate Biology, University of Kansas, Overland Park, KS; [3]Center for C. elegans Anatomy, Albert Einstein College of Medicine, Bronx, NY.

Correspondence to Matthew Buechner: buechner@ku.edu.

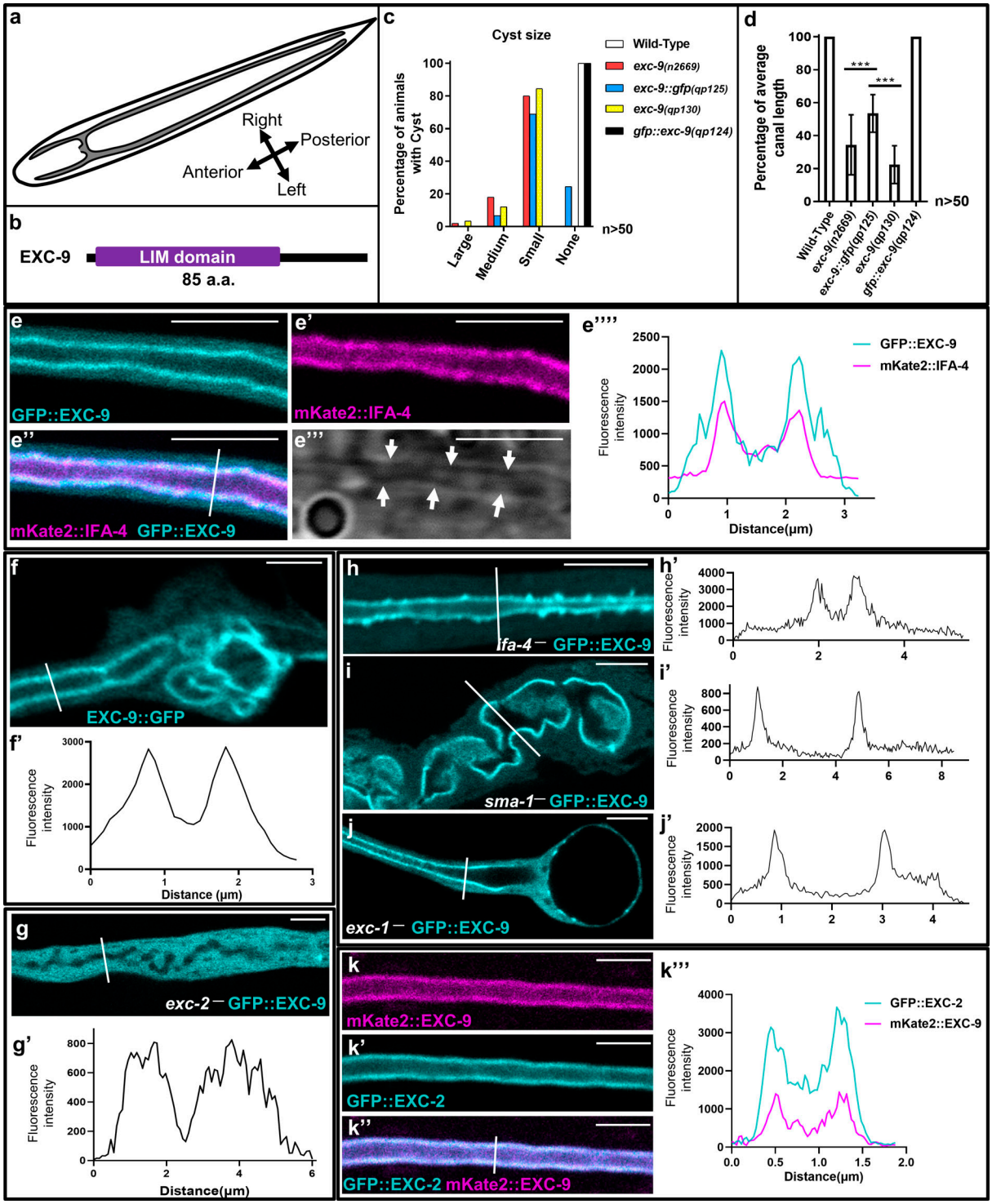

Figure 1. **EXC-9 is localized to the apical luminal surface of the excretory canals by intermediate filament protein EXC-2. (a)** Layout of *C. elegans* excretory canals and canal cell body within the animal. **(b)** Diagram of EXC-9 domains. **(c and d)** Comparison of maximum canal cyst size (c) and mean canal length ± SD (d) for different alleles of *exc-9*; $n > 50$. ***, $P < 0.001$, calculated via one-way ANOVA. **(e–e'''')** Collocation of GFP::EXC-9 and labeled intermediate filament mKate2::IFA-4 at the canal apical surface. GFP::EXC-9 expression at canal lumen and cytoplasm (e); mKate2::IFA-4 (e'); merge (e''); DIC micrograph of same section of canal (arrows indicate luminal surface, e'''); and fluorescence intensity profiles of EXC-9 (green) and IFA-4 (red) along white line in panel e''' (e''''). $n = 30$ animals examined. **(f and f')** The *qpIs125*(*exc-9::gfp*) allele allows cysts to form but is still retained apically (f); fluorescence intensity profile of EXC-9::GFP along white line in panel f (f'). $n = 30$ animals examined. **(g–j')** Expression of GFP::EXC-9 in homozygous mutants affecting canal apical structure. Fluorescence intensity profile along white lines for each mutant (g'–j'); *exc-2*⁻ ($n = 50$, g); *ifa-4*⁻ ($n = 25$, h); *sma-1*⁻ ($n = 25$, i); and *exc-1*⁻ ($n = 25$, j). **(k–k''')** Co-expression of mKate2::EXC-9 and GFP::EXC-2. mKate2::EXC-9 (k); GFP::EXC-2 (k'); merge (k''); and fluorescence intensity profiles of EXC-9 (green) and IFA-4 (red) along white line in panel k'' (k'''). All scale bars, 5 μm.

act in a genetic pathway to regulate canal morphology: EXC-9/CRIP1, EXC-1/IRG, and EXC-5/FGD (Grussendorf et al., 2016; Mattingly and Buechner, 2011; Tong and Buechner, 2008). All of the three encoded proteins have close human homologues: CRIP1 increases metastatic transformation and invasiveness in cell culture (Cousins and Lanningham-Foster, 2000; He et al., 2017; Li et al., 2017; Zhang et al., 2018); IRGM is involved with autophagy and pathogenic responses (Howard et al., 2011; Kumar et al., 2018; Pilla-Moffett et al., 2016); and FGD genes are loci of the developmental diseases Aarskog-Scott syndrome and Charcot-Marie-Tooth disease type 4H (Delague et al., 2007; Gao et al., 2001; Stendel et al., 2007). Mutants in these nematode genes show similar cystic defects in the structure of the canal apical surface as well as defects in vesicle transport: buildup of RAB-5–labeled vesicles and loss of RME-1–labeled vesicles in areas of cystic dilation (Grussendorf et al., 2016; Mattingly and Buechner, 2011). In addition, overexpression of any of these three genes results in a normal-diameter lumen (apical surface) folded up within a severely shortened canal. We interpreted these results as supporting a model in which EXC-9, EXC-1, and EXC-5 act in sequence to promote vesicle trafficking to the apical surface of the excretory cell, allowing that surface to be remodeled as the canals extend and widen during animal growth. It remains unknown, however, how EXC-9, EXC-1, and EXC-5 affect vesicle trafficking and whether cytoskeletal elements are involved with this process.

Here, we show that one of the three canal intermediate filament proteins, EXC-2, retains EXC-9/CRIP to the canal apical surface, mediated by the C-terminal domain (CTD) of EXC-2. The results also show that the EXC-1/IRG protein is retained at the apical surface of the canals independent of its binding partner EXC-9/CRIP and of intermediate filament EXC-2. Finally, overexpression of the vesicle trafficking protein RAB-8 partially suppresses the effects of mutations in *exc-9* and *exc-1* (but not mutations in *exc-5*) on the development of narrow canal tubules. These results delineate a novel pathway from the intermediate filament matrix to vesicle trafficking proteins that regulate the formation of the luminal diameter in this highly regulated polarized tubule cell.

Results

EXC-9 is localized to the apical surface of excretory canals by expression of EXC-2

EXC-9 (Human CRIP1 orthologue) is a small protein required for development and maintenance of the excretory canals; mutants develop shortened canals with large fluid-filled cysts (Tong and Buechner, 2008). The 85 amino acids of EXC-9 encode a single conserved LIM domain of the cysteine-rich protein class (Davis et al., 1998; Smith et al., 2010) at the N-terminus (60 amino acids; Fig. 1 b) followed by a short tail of unknown function conserved from nematodes to humans. In the *exc-9*(*n2669*) mutant, cystic canals always form a medium-sized (1/4–1/2 the diameter of the animal) cyst at the distal ends of the lumen, though cyst size and canal length vary depending on the allele used (Fig. 1, c and d). Allele *n2669* is a strong allele that was previously studied (Tong and Buechner, 2008). Allele *qp130*, a putative null CRISPR/Cas9–induced deletion of the first eight nucleotides of the coding region (the next ATG is not in-frame), produces significantly shorter canals than seen in *n2669* homozygotes, while insertion of GFP at the C-terminus of the protein (see below) creates a milder mutant phenotype, with smaller cysts and longer canals.

To determine the subcellular location of EXC-9, the CRISPR/Cas9 system was used to insert the *gfp* coding region at either the 5′- or -3′ terminus of *exc-9* (Dickinson et al., 2015). Expression of N-terminal GFP::EXC-9 (BK583) allowed the protein to remain fully functional and form long, thin, hollow canals, with the protein located predominantly at the apical surface (Fig. 1 e). Expression was also seen at lower levels within the uterine seam cell, both distal tip cells, and the lumbar ganglion (Fig. S1). Within the canals, expression was largely coincident with the intermediate filament protein marker mKate2::IFA-4, which labels the terminal web surrounding the canal lumen (Al-Hashimi et al., 2018), though some EXC-9 was also found within the cell cytoplasm. As noted above, when GFP was inserted at the C-terminus (BK589), the function of EXC-9 was compromised (Fig. 1, d and f). However, EXC-9::GFP was still enriched at the apical surface. Blockage of the C-terminal tail by GFP impaired EXC-9 function without affecting apical localization.

As EXC-9 has no transmembrane domain but is enriched at the apical membrane, we examined how EXC-9 is retained at the membrane by crossing our fully functional GFP::EXC-9 strain to mutants defective in known canal apical lumen cytoskeletal proteins (Fig. 1, g–j). In the absence of the large intermediate filament protein EXC-2 (Al-Hashimi et al., 2018), GFP::EXC-9 lost apical localization and became evenly distributed throughout the canal cytoplasm (Fig. 1 g). In contrast, loss of another canal-specific intermediate filament, IFA-4 (Flibotte et al., 2010), which likely forms heterodimers with EXC-2, did not affect EXC-9's ability to be retained at the apical surface (Fig. 1 h). Similarly, loss of β_H spectrin SMA-1 causes formation of large irregular cysts throughout the length of the canals (Buechner et al., 1999) but retains strong expression of EXC-9 predominantly at the apical surface (Fig. 1 i). Finally, loss of the IRG GTPase protein EXC-1, a known EXC-9 binding partner (Grussendorf et al., 2016), also had no effect on the apical retention of EXC-9 (Fig. 1 j). The results indicate that EXC-2 retains the majority of EXC-9 protein at the apical surface; this was confirmed by coexpression of functional labeled EXC-2 and EXC-9, which were completely collocated at the canal apical surface (Fig. 1 k).

EXC-2 CTD localizes EXC-9 to the apical surface

Intermediate filaments usually consist of a short N-terminal domain (NTD) and a longer CTD flanking a conserved filament domain used for dimerization (Herrmann and Aebi, 2016). While IFA-4 and IFB-1 follow this plan (including a conserved lamin tail domain [LTD] within the CTD; Carberry et al., 2009; Zuela and Gruenbaum, 2016), EXC-2 has a much longer NTD and no lamin tail homology in its CTD (Fig. 2 a). There is also a gene termed *ifc-2* (Hüsken et al., 2008) that begins from a promoter in an exon of *exc-2* and that contains only the filament domain and CTD, but isoforms of IFC-2 are found predominantly in the

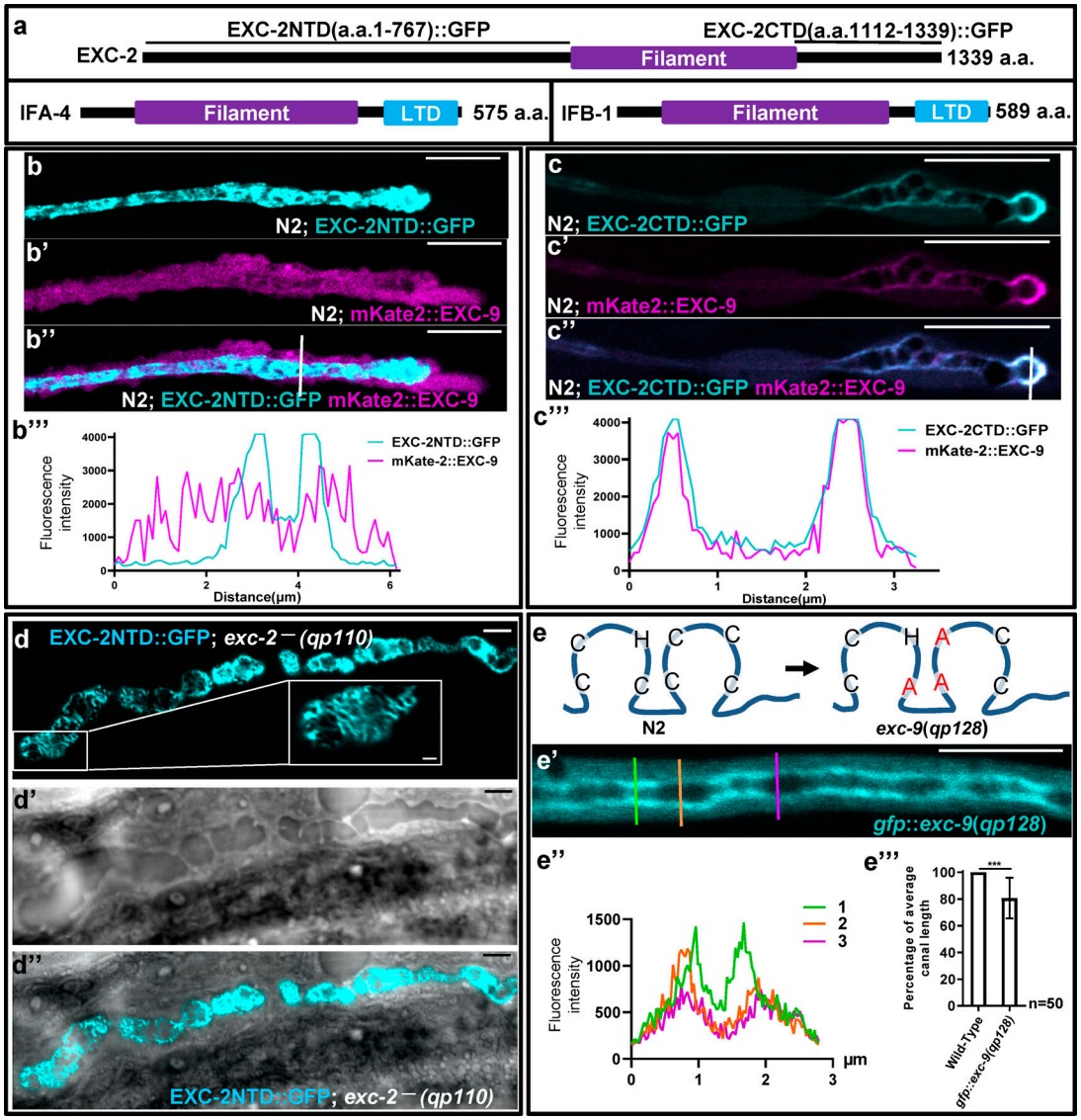

Figure 2. **EXC-2 C-terminal fragment is colocalized with EXC-9 to the canal apical membrane. (a)** Scale diagram of domains of intermediate filament expressed in the excretory cell, including EXC-2, IFB-1, and IFA-4. The lamin-like intermediate filament domain allows homo- and hetero-dimerization of the filaments. **(b–b''')** Overexpression of EXC-2(1–767; N-terminal half) in BK590 (EXC-9 modified via CRISPR/Cas9 insertion of mKate2) reduced binding of mKate::EXC-9 to the apical surface. Overexpressing EXC-2(1–767) fluorescence (b); EXC-9 fluorescence (b'); merge (b''); and fluorescence intensity profiles of EXC-2(1–767) (green) and EXC-9 (red) along white line indicated in b'' (b'''). *n* = 29 animals examined. **(c–c''')** Overexpressing EXC-2 (1112–1339) in BK590 (mKate2::EXC-9) showed colocalization of both proteins to the growing tip of the luminal canal surface; EXC-2(1112–1339) (C-terminal portion) fluorescence (c); EXC-9 fluorescence (c'); merge (c''); and fluorescence intensity profiles of EXC-2(1–767) (green) and EXC-9 (red) at the canal tip along the white line indicated in c'' (c'''). (*n* = 25 animals). **(d–d'')** EXC-2(1–767) overexpressed in *exc-2*(*qp110*) homozygotes forms a meshwork at the canal apical surface. EXC-2 fluorescence, inset at 2× magnification (d); DIC image showing cystic lumen (d'); merge (d''). (*n* = 32 animals). **(e–e''')** Mutation of the LIM domain prevents EXC-9 localization to the apical surface. Diagram of EXC-9 showing conserved cysteines (C) and histidine (H) in loops of LIM domain. Amino acids in red indicate replacement by alanine (A) in mutant strain (e); EXC-9 fluorescence in cysteine-substituted mutant is evenly expressed throughout the cytoplasm surrounding an enlarged lumen (e'); fluorescence intensity profile along three lines in e' (*n* = 26 animals, e''); comparison of canal length ± SD in the *exc-9*(*qp128*) mutant (3 Cys→Ala) to that in wild-type (e'''). ***, P < 0.001 (*n* = 50). All scale bars, 5 μm.

intestine and are not expressed in the canal cell (Geisler et al., 2020).

To determine which section of EXC-2 is required for binding EXC-9 to the luminal surface, the long NTD (amino acids 1–767) and short CTD (amino acids 1112–1339) were each cloned into a fluorescence translational construct for overexpression in wild-type and in the *exc-2*(*qp110*) null mutant background. In a previous study, overexpression of full-length *exc-2* PCR product greatly shortened the canals to less than half-length and caused small dilations of the lumen (lumen diameter <1/4 body width; Al-Hashimi et al., 2018). Here, overexpression of each of these partial *exc-2* constructs from the strong canal-specific *vha-1* promoter caused similarly shortened canals with small dilations (Fig. 2, b and c). In the wild-type background, overexpressed EXC-2NTD::GFP remained apically localized (Fig. 2 b), but labeled EXC-9 did not. The presence of excess EXC-2NTD

prevented EXC-9 from being retained at the luminal membrane. This implies that EXC-2NTD and EXC-9 compete for the same locations on the luminal membrane.

Overexpression of EXC-2CTD::GFP exhibited a unique polarized fluorescence phenotype (Fig. 2 c): canals were generally wild-type in diameter along their length, but did not grow to full length and terminated in medium-sized cysts at the distal ends. In addition, fluorescently labeled EXC-2CTD and labeled EXC-9 were fully collocated but strongly enriched toward the distal end, with very bright fluorescence at the distal tip of the canal lumen. We inferred that the CTD of EXC-2 recruits EXC-9 and that they are able to remain at high concentration at the canal apical surface only at the luminal tip of the canals.

In the *exc-2*(*qp110*) null allele mutant background, EXC-2NTD::GFP was still localized at the apical surface (Fig. 2 d), and its expression pattern resembled the localization and meshwork pattern of wild-type GFP::EXC-2 expressed in animals lacking one of the other intermediate filament proteins, IFB-1 or IFA-4 (Al-Hashimi et al., 2018). This indicated that the N-terminus of EXC-2NTD is capable of binding either to the other intermediate filament proteins IFB-1 and IFA-4 or to other proteins anchored or bound to the luminal surface.

GFP attachment to either end of the small EXC-9 protein did not affect its expression at the apical surface of the excretory canals, although C-terminal GFP impaired EXC-9 function (Fig. 1 d). We investigated the role of the LIM domain at the N-terminus of EXC-9 by using CRISPR/Cas9 to make endogenous mutations in key conserved cysteines (Fig. 2 e). LIM domains are composed of two contiguous zinc fingers containing three conserved cysteine residues and one histidine in the first zinc finger and four conserved cysteines in the second zinc finger (Weiskirchen and Günther, 2003). We used CRISPR/Cas9 to replace the last cysteine in the first zinc finger and first two cysteines in the second zinc finger with alanine (Fig. 2 e). With these changes, about half of the animals (28 of 50) were mildly affected in regard to canal length, with canals reaching longer than half the length of the organism, while the other animals had full-length canals (81% of full-length average; Fig. 2 e'''). In the cysteine-substituted mutant canals, apical retention of labeled EXC-9 was variably impaired, with some sections showing wild-type levels of EXC-9 at the apical surface compared with the cytoplasm, while in others, almost no EXC-9 was retained at the apical surface. (Fig. 2 e') Loss of apical EXC-9 was coincident with areas of wider lumen, possibly nascent cysts. These results suggest that LIM domain function plays a role in apical localization of EXC-9 to the canal apical surface.

EXC-1 is also localized to the canal apical surface

EXC-9 binds to the N-terminal half of EXC-1 and acts genetically upstream of EXC-1 to mediate endosomal vesicle transport within the canals (Grussendorf et al., 2016). EXC-1 possesses two RAS-like GTPase domains and is the sole nematode homologue of mammalian IRG proteins (Fig. 3 a; Grussendorf et al., 2016). Since EXC-9 is largely collocated with EXC-2, we examined whether the EXC-9–binding partner EXC-1 is also retained near EXC-2 within the excretory cell. Through use of CRISPR/Cas9, GFP was inserted at the C-terminus of EXC-1. This labeled protein was found at the apical surface, and surprisingly, unlike EXC-9, little EXC-1 protein was apparent in the cytoplasm (Fig. 3 b). In addition to the excretory canal cell, EXC-1 was expressed at lower levels in the amphid sheath cells (Fig. S2). Localization of EXC-1 did not require activity of EXC-9, since in the deletion mutant *exc-9*(*qp130*), EXC-1 fully retained its localization to the apical luminal membrane (Fig. 3 c). Similarly, crossing the labeled EXC-1 strain into a null *exc-2*(*qp110*) mutant strain caused no change to the apical localization of EXC-1 (Fig. 3 d). EXC-1 appears to be anchored to the membrane independently of the EXC proteins that act genetically upstream of EXC-1.

SMA-1/spectrin is required for spacing of the EXC-2 meshwork

The β_H–spectrin SMA-1 is another important cytoskeletal element regulating canal shape (Buechner et al., 1999), but it does not affect the placement of EXC-9 (Fig. 1 i). β_H-spectrin and the ERM homologue ERM-1 anchor actin filaments to the apical surface (Khan et al., 2019, 2013; Praitis et al., 2005). In *erm-1* knockdown animals, labeled IFB-1 showed the intermediate filament network to be greatly disrupted (Khan et al., 2019). To investigate the ability of SMA-1 to affect placement of intermediate filaments, we examined the other two canal intermediate filaments via separately crossing the fluorescent *mKate2*::*ifa-4* and *gfp*::*exc-2* strains into animals carrying a null mutation either in *sma-1* or in *exc-4* (encoding a chloride intercellular channel ion channel, as a control mutant with large cysts), both of which also severely disrupt canal morphology (Berry et al., 2003; Praitis et al., 2005). In the homozygous *sma-1*(*ru18*) mutant background, both mKate2::IFA-4 and GFP::EXC-2 fluorescence showed disruption to the spacing of filaments surrounding the apical surface (Fig. 4, b and d). The "weave" of the intermediate filament meshwork was looser, allowing the appearance of large gaps of open membrane between intermediate filaments, as seen by the repetitive distance between peaks of fluorescence (Fig. 4, b' and d'). In contrast, in the *exc-4* background (Fig. 4, c and e), the meshwork of both labeled filaments generally showed a tighter weave, with filaments aligned closely to each other, comparable to the meshwork of wild-type animals (Fig. 4, a and a''), even though *exc-4* animals exhibit very large canal cysts comparable in size to those of *sma-1* mutants (Buechner et al., 1999). Occasional filament breakdowns in very large cysts could be seen in *exc-4* mutant animals, but the background filament weave was generally as tight as in wild-type animals. The disruption of filament weave in *sma-1* mutants is similar to that caused by knockdown of ERM-1 (Khan et al., 2019). We conclude that both ERM-1 and SMA-1 are needed for proper layout of the intermediate filament network.

Examination of *sma-1* and *exc-4* mutants by means of electron microscopy (Fig. 5) showed further differences between these animals. In the *exc-4*(*rh133*) mutant, the luminal surface electron-dense terminal web was intact and associated tightly with the membrane at the luminal surface (Fig. 5 c), as is seen in wild-type animals (Fig. 5 a). The membrane itself was in contact with long chains of small canalicular vesicles (Fig. 5, a and c, marked by asterisks), rich in vacuolar ATPase and aquaporin, and which pump water into the canal lumen for expulsion from the animal

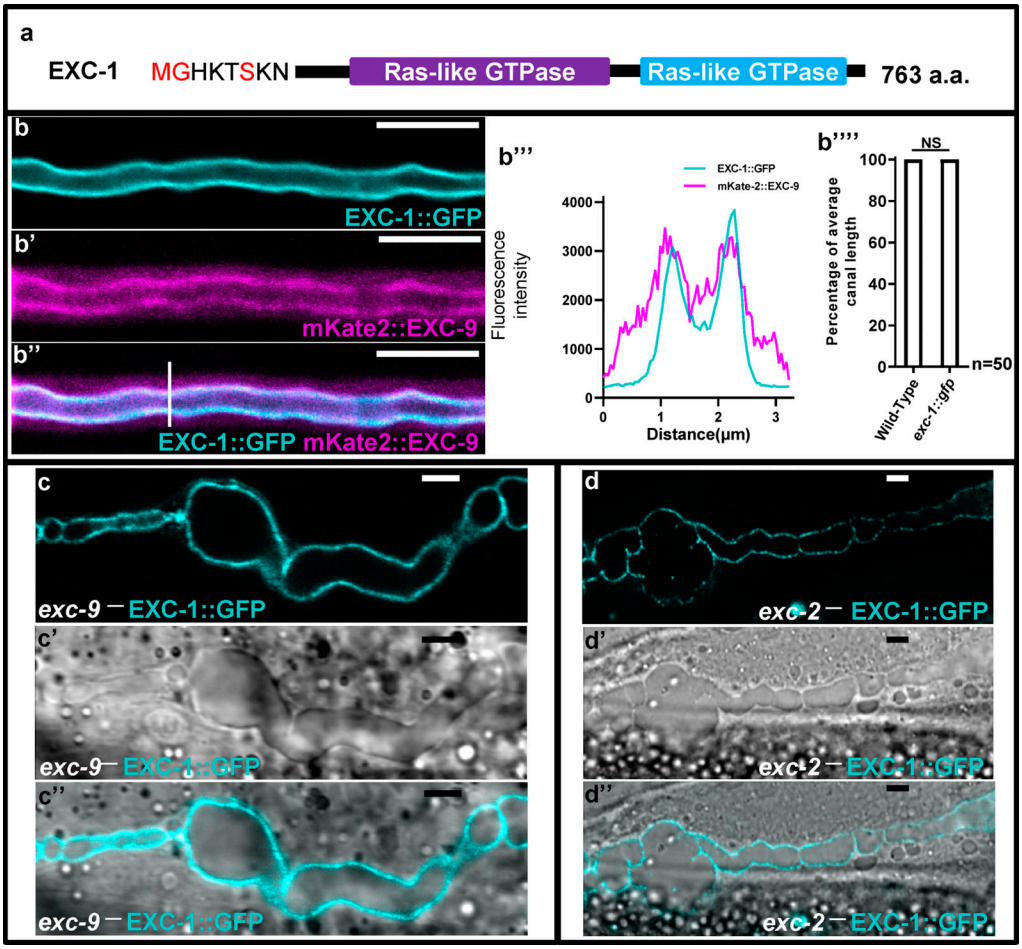

Figure 3. **EXC-1/IRG is localized exclusively at the apical surface of canals. (a)** Scale diagram of the GTPase domains within the EXC-1 protein. **(b–b'')** Collocation of (CRISPR/Cas9–generated endogenous) EXC-1::GFP and mKate2::EXC-9 at the canal apical surface. EXC-1 fluorescence (b); EXC-9 fluorescence (b'); and merge (b''). **(b''')** Fluorescence intensity profiles of mKate2::EXC-9 (red) and EXC-1::GFP (green) along the white line of b''. **(b'''')** Comparison of average canal length of wild-type and *exc-1::gfp* animals. For fluorescence studies, *n* = 20 animals examined; for canal length, *n* = 50 animals examined. **(c–c'')** EXC-1::GFP remains at the apical surface in a homozygous null *exc-9(qp130)* cystic mutant. EXC-1 fluorescence (c); DIC image of fluid-filled cysts (c'); and merge (c''); *n* = 25 animals examined. **(d)** EXC-1 is retained at the surface of canals in a homozygous *exc-2(qp110)* cystic mutant. EXC-1 fluorescence (d); DIC image of fluid-filled cysts (d'); and merge (d''); *n* = 25 animals examined. All scale bars, 5 µm.

(Sundaram and Buechner, 2016). In contrast, the *sma-1(e30)* mutant (Fig. 5 d) exhibited an electron-dense terminal web layer that was no longer juxtaposed to the apical membrane. In addition, the terminal web was broken in places, with large gaps between electron-dense areas (arrowheads in Fig. 5 d'). Although canalicular vesicles were numerous in this mutant, the canalicular membrane appeared disorganized in areas where the terminal web was distant from the membrane. Finally, in the *exc-2(rh90)* mutant missing the largest intermediate filament protein, the terminal web was largely missing from some areas of the apical membrane, and very few canalicular vesicles were visible, as seen in Fig. 5 b, although some areas of the canal in *exc-2(rh90)* and *exc-2(rh209)* animals retained some terminal web together with canaliculi attached, as reported previously (Al-Hashimi et al., 2018; Buechner et al., 1999). These results confirm that intermediate filaments make up the terminal web of the excretory canal, similar to terminal webs in the gut (Coch and Leube, 2016), and that β_H-spectrin is required for proper arrangement of these intermediate filaments. In addition, the terminal web appears to be necessary for stabilization of the network of canalicular vesicles that are presumed to carry out osmoregulation of the animal in hypotonic environments.

Apical actin filaments are bundled in *exc-1*, *exc-5*, and *exc-9* mutants

Previous data showed that EXC-9, EXC-1, and EXC-5 act in sequence to regulate endosomal vesicle transport in the excretory canals (Grussendorf et al., 2016; Mattingly and Buechner, 2011; Tong and Buechner, 2008). To investigate the potential cargo or cytoskeletal protein being regulated, we used a strain containing two integrated constructs that both use a canal-specific promoter to express either a cytoplasmic CFP or the actin dye LifeAct (Shaye and Greenwald, 2015). To better visualize the full length of actin filaments along the curved apical surface of the canals, a series of Z-axis pictures were taken and merged into a single micrograph (Fig. 6 a). In the wild-type canal background (Fig. 6 b), the apical membrane actin filaments appear as a uniform field of short actin filaments throughout the length of

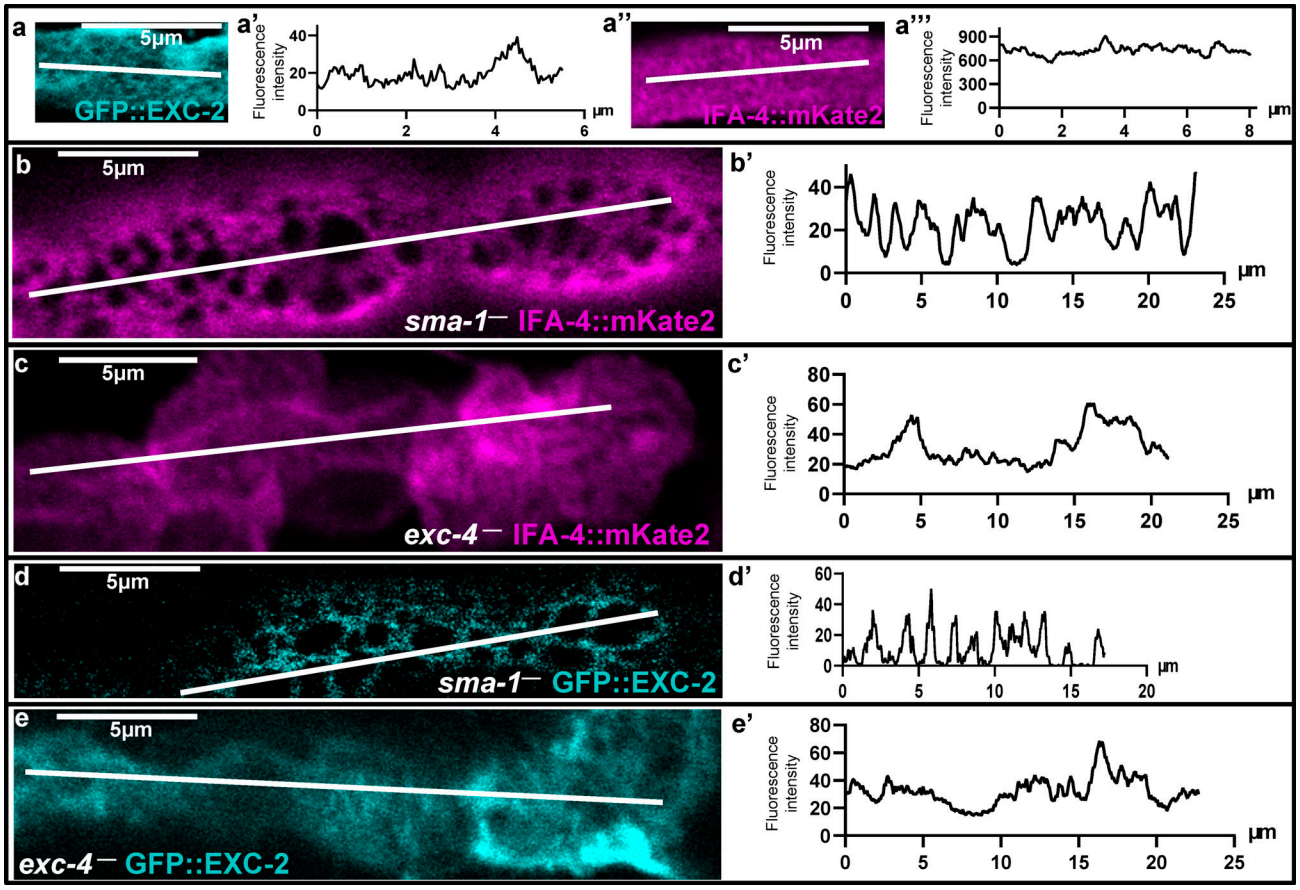

Figure 4. **SMA-1 is required for proper intermediate filament arrangement. (a and a'')** Fluorescence of labeled EXC-2 (n = 20) and IFA-4 (n = 20) in wild-type background. **(a' and a''')** Fluorescence intensity profile along the white line in the corresponding micrograph. **(b–e)** Fluorescence of labeled IFA-4 or EXC-2 in homozygous *sma-1* or *exc-4* backgrounds. **(b'–e')** Fluorescence intensity profile along the white line in the corresponding micrograph. **(b)** IFA-4 fluorescence in *sma-1*(*ru18*) homozygous mutants (n = 25 animals examined). **(c)** IFA-4 fluorescence in *exc-4*(*rh133*) mutants (n = 25 animals). **(d)** EXC-2 fluorescence in *sma-1*(*ru18*) mutants (n = 25 animals). **(e)** EXC-2 fluorescence in *exc-4*(*rh133*) mutants (n = 25 animals).

the canal apical surface. This structure is maintained in the *sma-1* mutant (Fig. 6 c), where the canal lumen is often enlarged to a similar degree throughout the canal without obvious septations (Buechner, 1999); this result suggests that the labeled actin filaments are anchored to the membrane by another means. In the *exc-9* mutant background, some aggregation of actin filaments into thick bundles (Fig. 6 d, arrow) became evident in areas with larger septate cysts, corresponding to septate cysts that thin the amount of cytoplasm present. This effect was progressively exacerbated in *exc-1* mutants (Fig. 6 e) and most dramatically in the large cysts of *exc-5* mutants, where the actin filaments contained little actin except in thick bundles (Fig. 6 f). In addition, in the *exc-5* mutant, these thick bundles were collocated with accumulations of cytoplasmic material around the swollen luminal cyst. We conclude that these three *exc* mutants therefore are needed to stabilize a uniform actin meshwork at the apical surface.

EXC-1 and EXC-9 promote RAB-mediated apical transport

In *exc-1*, *exc-5*, and *exc-9* mutants, endosomal expression of the basal trafficking marker RME-1 was significantly decreased within the cytoplasm of canal cysts, while that of other vesicular markers, especially the early endosome antigen EEA-1 and (to a lesser extent) the apical trafficking marker RAB-11.1, were increased (Grussendorf et al., 2016; Mattingly and Buechner, 2011). To better understand the relationship of these EXC proteins on traffic movement within the excretory canal, we first examined competition between apical and basal traffic markers (Fig. 7, a–c). A strain carrying a stable integrant of *mCherry::rme-1* driven by a canal-specific promoter (Mattingly and Buechner, 2011) exhibited punctate endosomes and strong cytoplasmic expression (Fig. 7 a). We crossed this marker line to a strain harboring an integration of a construct that strongly expresses canal-specific *gfp::rab-11.1* (Fig. 7 b). With the expression of *rab-11.1*, expression of mCherry::RME-1 in the canal was greatly reduced to near-background levels (Fig. 7 c). We conclude that apical and basal transport within the excretory canal cell depends on the ratio of apical-directed and basal-directed transport machinery present.

Next, since expression of Rab proteins within the canal appears to affect transport ratios, as in the intestine (Sato et al., 2014), and *exc-9*, *exc-1*, and *exc-5* mutants impair vesicle trafficking and maintenance of the apical surface (Grussendorf

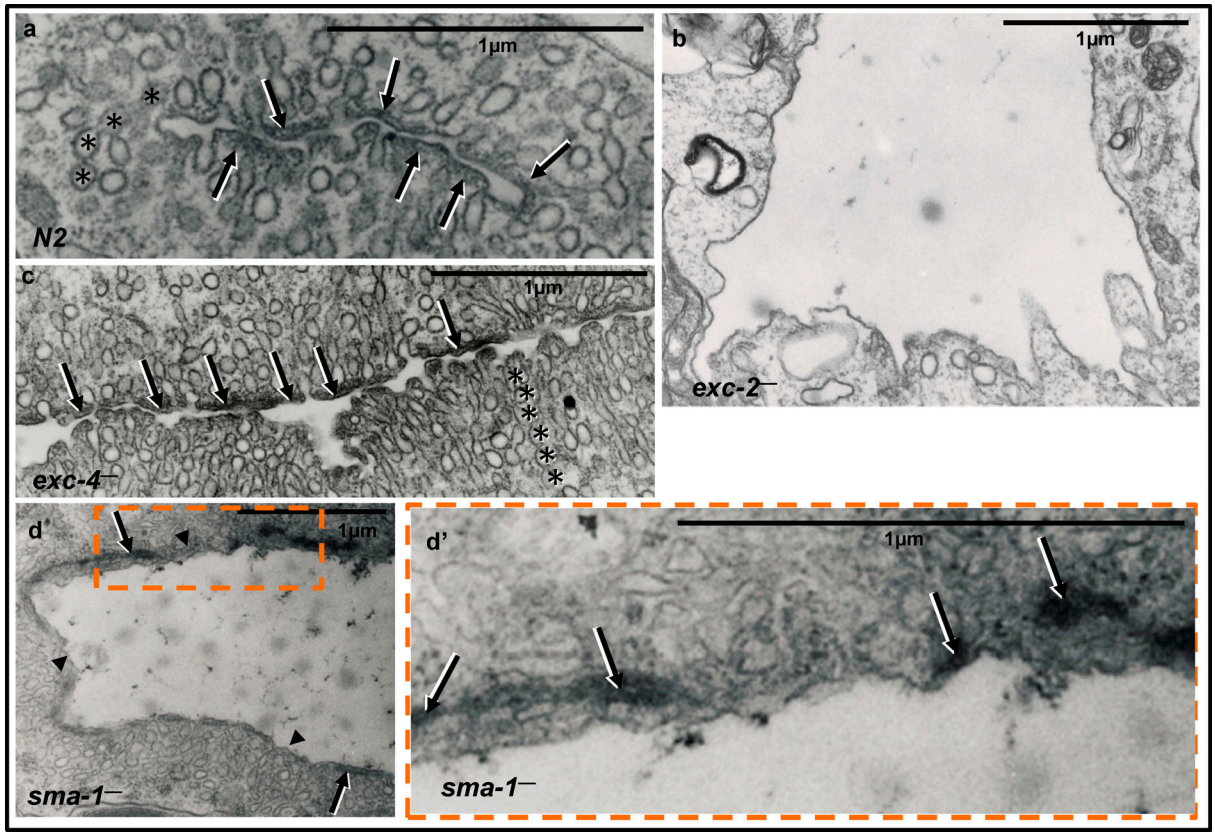

Figure 5. **Transmission electron micrographs of cross section of canals in wild-type and homozygous mutant animals. (a–c)** N2 wild type (a); *exc-2* (*rh90*) mutant (b); and *exc-4*(*rh133*) mutant (c); electron-dense intermediate filament–rich terminal web (arrows) is closely apposed to the apical membrane, and canalicular vesicles (asterisks) are connected to the lumen and to each other (n = 3 animals, multiple sections each). In large cyst of *exc-2*(*rh90*) mutant (b), the terminal web is missing, as is the bulk of canalicular vesicles. **(d)** *sma-1*(*e30*) mutant shows frequent detachment of the terminal web (arrows) from the apical membrane, with visible gaps (arrowheads) between sections of the terminal web (n = 6 animals, multiple sections). **(d')** Enlargement of boxed section of d; in spite of terminal web disruption, abundant canalicular membrane is visible, though the vesicles appear disrupted in areas where the terminal web is separated from the membrane.

et al., 2016; Mattingly and Buechner, 2011; Tong and Buechner, 2008), we examined whether overexpression of an apical-directed Rab protein could rescue mutation of the *exc-1*, *exc-5*, and *exc-9* genes (Fig. 7, d and e). A construct overexpressing canal-specific *rab-8* was injected into *exc-1* (*rh26*), *exc-5* (*rh232*), and *exc-9*(*qp130*) mutants (Fig. 7, d–f). Cyst formation in these mutants causes significant shortening of the canals, but in the presence of excess RAB-8, the canals of *exc-1* and *exc-9* mutants were significantly longer (Fig. 7 d). Similarly, overexpression of any of these *exc* genes caused the canals to have a "convoluted" phenotype, where the basal surface was shortened, while the normal-diameter luminal surface was still extended and ended up coiled within the canal (Tong and Buechner, 2008; Fig. 7 e). Canal overexpression of *rab-8* also caused a significant increase in convoluted canals in *exc-1* and *exc-9* mutants (though not as strong as overexpression of the *exc* proteins themselves; Grussendorf et al., 2016; Fig. 7 f). Surprisingly, overexpression of *rab-8* had no significant effect on the *exc-5* mutant, either in canal length or formation of cystic canals (Fig. 7, d and f). These genetic epistasis experiments suggest that RAB-8 acts downstream of EXC-9 and EXC-1 in directing cargo to the apical surface.

Discussion

Intermediate filament EXC-2 retains EXC-9/CRIP at the apical surface

The cytoskeleton forms and reinforces the shape of cells. Projections of actin and microtubules underlie cell protrusions, while intermediate filaments act as ropes or stretchable bungee cords to allow limited stretch to the plasma membrane and nuclei (Delacour et al., 2016; Gerace and Burke, 1988; Gruenbaum and Foisner, 2015). Both of these elements are needed for formation of long hollow tubules, which must be guided to grow out along the length of the body wall, but whose luminal diameter must be restrained as excess water is brought into the tubule to be expelled from the organism (Sundaram and Buechner, 2016; Sundaram and Cohen, 2017). The results in this paper show that EXC-1/IRG GTPase and EXC-9/CRIP1 are both held predominantly near the apical surface, either in the plasma membrane itself or together with the EXC-2/IFA-4/IFB-1 intermediate filaments of the terminal web surrounding the lumen. EXC-1 is located at the apical surface even in *exc-2* mutants where there is little or no terminal web (Fig. 3). Upon re-examining the amino acid sequence of EXC-1 with the help of predictive lipidation tools, we found that its N-terminus

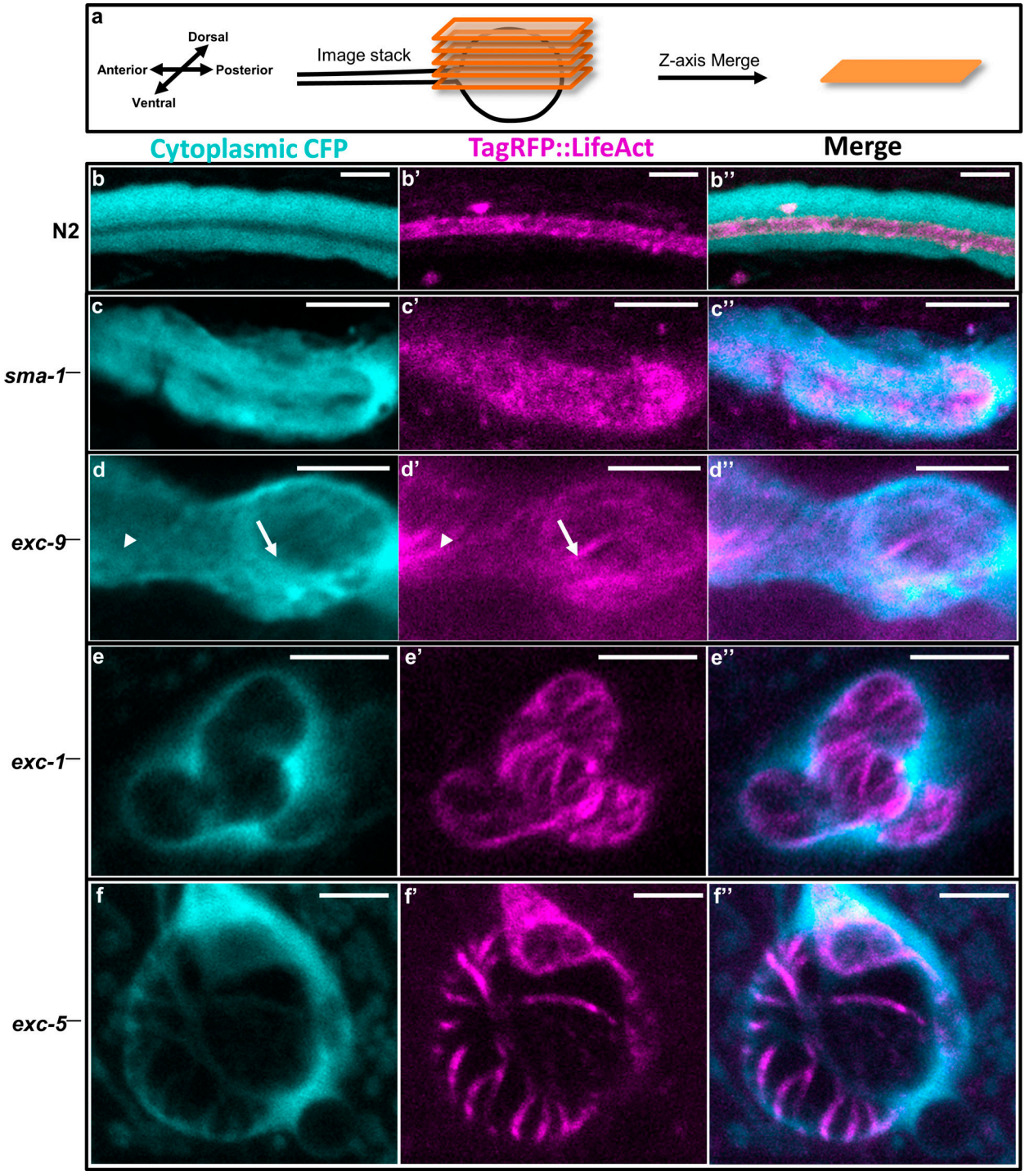

Figure 6. **Actin filament mesh exhibits increasingly severe bundling gaps in *exc-9*, *exc-1*, and *exc-5* mutants. (a)** Scheme of summation of fluorescence through Z-stack serial pictures through half the depth (nearest to hypodermis and microscope objective) of canals and cysts to show filament morphology of LifeAct-labeled filaments at the canal apical surface. **(b–f'')** All animals express cytoplasmic CFP under an integrated canal-specific promoter and an over-expressing construct of fluorescent actin label (LifeAct) under the same promoter. Left column: cytoplasmic fluorescence; center column, actin filament mesh; right column, merge. **(b–d)** Wild-type background (b); homozygous *sma-1*(*ru18*) background (c); and homozygous *exc-9*(*n2669*) background (d); arrows indicate a distinct thickly bundled actin filament, while arrowheads indicate a less distinct actin bundle. **(e)** Homozygous *exc-1*(*rh26*) background. **(f)** Homozygous *exc-5*(*rh232*) background. All scale bars, 5 µm. $n \geq 20$ for all samples.

contains a cotranslational myristoylation sequence MGHKTS (Johnson et al., 1994; Udenwobele et al., 2017; Xie et al., 2016). Our attempts to engineer a CRISPR/Cas9-mediated insertion of GFP at the N-terminus of this protein were unsuccessful, which may indicate that this sequence is essential for organismal viability. Future biochemical studies of possible lipidation of this

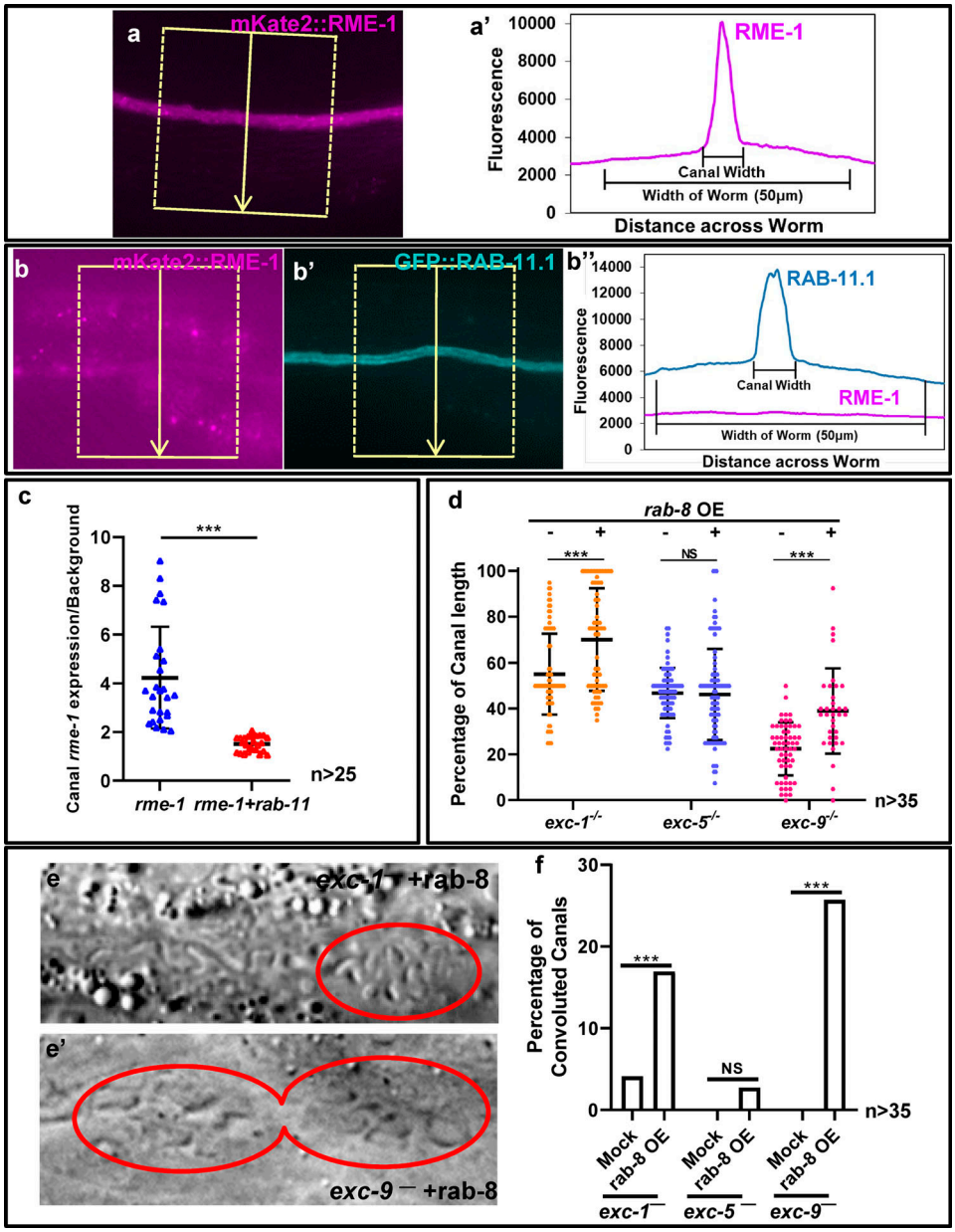

Figure 7. **EXC-1 and EXC-9 promote RAB-mediated apical transport. (a and a')** mCherry::RME-1 is overexpressed in the excretory canals. Fluorescence micrograph of section of excretory canal expressing *mCherry::rme-1* construct under an *exc-9* promoter; endosomes are visible as bright puncta (a); measurement of fluorescence in boxed area of panel a, measured in direction of arrow along line in panel, with a width of 300 pixels (space between dotted lines; a'). **(b–b'')** Expression of GFP::RAB-11 in worms also expressing mCherry::RME-1. Fluorescence micrograph (b); fluorescence of mCherry::RME-1; area measured is shown in box (b'); and fluorescence intensity of GFP::RAB-11 and mCherry::RME-1 (b''). **(c)** Graph of average ratio of fluorescence of mCherry::RME-1 to autofluorescence within worm in area of canal. Left column: average ratio for animals expressing fluorescent mCherry::RME-1 alone; right column: for animals expressing GFP::RAB-11 in addition to mCherry::RME-1; $n > 25$ animals for each column. All data points are shown, including the mean ± SD. ***, $P < 0.001$ as calculated via one-way ANOVA test. **(d)** Length of excretory canals of *exc* mutant animals and same strain overexpressing *rab-8*; posterior canal lengths were measured. All data points are shown, including the mean ± SD. ***, $P < 0.001$; P value is calculated via one-way ANOVA test. **(e and e')** Convoluted canal phenotype in *exc-1* and *exc-9* mutant animals with overexpression of *rab-8*. *exc-1*$^{-/-}$ (e); *exc-9*$^{-/-}$ (e'). Circled areas show regions of normal-diameter lumen coiled within shortened, swollen cytoplasm. **(f)** Measurement of frequency of canals showing convoluted tubules trapped within shortened basal surface; a convolution is defined as the lumen crossing itself at least once. Convolutions were counted in the progeny of animals microinjected with buffer (Mock) and for animals overexpressing *rab-8*. ***, $P < 0.001$; P value is calculated by one-way ANOVA test. $n > 35$ for all samples in d and f. OE, overexpressing.

protein should be fruitful for further understanding its interactions with cytoskeletal elements.

EXC-9 is a small protein containing only a single LIM domain and a short tail and was expected to be fully cytoplasmic. It was highly surprising to find that this protein was instead found to be predominantly concentrated at the terminal web at the apical surface, though with a visible fraction in the cytoplasm (Fig. 1). Also surprising was the finding that, of the three intermediate filament proteins within the excretory canal, EXC-2 is specifically needed to retain EXC-9 at the terminal web (Fig. 1). These

results suggest that EXC-9 is either present in the cytoplasm before being bound to the terminal web, or it can be released into the cytoplasm from the terminal web. Impairment of the EXC-9 LIM domain (Fig. 2) reduced the ability of EXC-9 to bind to the terminal web, with regions of lower terminal web fluorescence associated with lumen widening, possibly indicative of formation of incipient cysts. These observations reinforce the idea that EXC-9 binding to the canal terminal web is important for maintaining the narrow diameter of the excretory canals. The effect of mutation of the LIM domain was surprisingly small, however, compared with that of null mutants of *exc-9*. It is possible that the C-terminal domain of EXC-9 could be most critical for the function of this protein or instead that the mutated LIM domain retained some residual binding ability.

Overexpressed labeled EXC-2 (intermediate filament) NTD appeared along the entire canal length and largely prevented EXC-9 from binding to the terminal web, resulting in EXC-9 being essentially all cytoplasmic. In contrast, overexpression of the EXC-2 CTD lowered the amount of free EXC-9 visible in the cytoplasm and concentrated this protein at the terminal web toward the cystic posterior end and especially at the canal tip (Fig. 2). The canal luminal surface extends the length of the animal, closely following the growing tip of the basal surface during embryogenesis and the first larval stage (Fujita et al., 2003). For overexpressed EXC-2 CTD and EXC-9 to label only the canal luminal tip and cystic areas, CTD must accumulate there until a step occurs to restrain dilation of the membrane, presumably via vesicle trafficking and construction of the actin cytoskeleton and terminal web.

There are 11 cytosolic intermediate filaments in *C. elegans* (Carberry et al., 2009; Dodemont et al., 1994; Karabinos et al., 2001; Zuela and Gruenbaum, 2016). Several studies have focused on the intestinal terminal web, where intermediate filaments are also necessary to maintain narrow luminal diameter (Coch and Leube, 2016; Geisler et al., 2020; Karabinos, 2019; Karabinos et al., 2017; Khan et al., 2013, 2019). While *exc-9* and *exc-1* are not expressed within the intestine, other LIM-domain proteins could be interacting with intermediate filaments in this tissue. EXC-1, EXC-9, and its homologue VALV-1 are expressed in a range of tissues that undergo stretching and bending movements, including the intestinal-pharyngeal valve, spermathecal valves, and amphid glia (Grussendorf et al., 2016; Tong and Buechner, 2008).

Interactions with the actin cytoskeleton

Mutants in *sma-1* (encoding β_H spectrin) show disorganization of the terminal web (Fig. 4 and Fig. 5; Buechner et al., 1999; Praitis et al., 2005), which indicates that this spectrin has an organizing effect on the intermediate filament network, though the *sma-1* mutation does not abrogate the terminal web's overall formation near the apical membrane. Significantly, *sma-1* mutants tend to exhibit very wide canals with few narrow septations, with numerous canaliculi attached to the apical membrane (Fig. 5 d), unlike mutants of intermediate filament genes (Fig. 5 b; Al-Hashimi et al., 2018; Khan et al., 2019; Kolotuev et al., 2013). The presence of intermediate filaments at the apical membrane therefore appears to be necessary for attachment of these canaliculi, as much as the activity of the exocyst and STRIPAK complex is (Armenti et al., 2014; Lant et al., 2015).

Loss of EXC-9, EXC-1, or EXC-5 function resulted in ACT-5 actin filaments appearing as thick cables restraining the lumen, which swelled into cysts around these cables (Fig. 6). Surprisingly, *sma-1* mutants lacking β_H-spectrin still maintained a tightly knit meshwork of actin around the canal lumen, which suggests that unlike the FERM-domain protein ERM-1 (Khan et al., 2013, 2019), this spectrin is not the most critical organizer of these actin filaments. This result was surprising, since SMA-1 regulates actomyosin cytoskeletal contractility in several *C. elegans* tissues (Wirshing and Cram, 2018). Disorganization of the terminal web could therefore be secondary to SMA-1's effects on cytoskeletal actin, or perhaps actomyosin contractility may not play a significant role in organizing the canal actin meshwork.

Interactions with Rab proteins

EXC-9 acts genetically upstream of and binds to EXC-1, which itself acts upstream of EXC-5. Results here show that overexpressing RAB-8 partially rescues the *exc-9* and *exc-1* mutants, but not the *exc-5* mutants (Fig. 7). While the result is consistent with RAB-8 acting downstream of EXC-9 and EXC-1, overexpression of these two genes by themselves gives stronger rescue (Grussendorf et al., 2016; Tong and Buechner, 2008), suggesting that EXC-9 and EXC-1 may stimulate multiple trafficking proteins. Both RAB-11.1 and RAB-8 target vesicles to the apical membrane (Sato et al., 2014), so they may be acting together downstream of EXC-1.

Rab8 has been seen to direct traffic apically and basolaterally in different organisms and cell types (Ang et al., 2003; Bellec et al., 2018; Sato et al., 2007), which complicates interpretation of our overexpression results. The *exc* mutants show clear defects in morphogenesis and maintenance of the apical surface, and overexpression of *exc* genes yields normal-diameter "convoluted" lumens within canals that are severely shortened on the basal surface. While RAB-8–directed cargo in vesicles inside the excretory canals has not been identified, overexpression of *rab-8* phenocopies the convoluted canals. This suggests that RAB-8 directs traffic to the apical surface in this cell type.

RAB-8 did not rescue the effects of *exc-5* mutation. This could indicate that RAB-8 acts upstream of EXC-5 (as in the model posited above), which is expressed at or near the canal apical surface (Mattingly and Buechner, 2011), or that RAB-8 stimulates a different guanine exchange factor while a different protein (perhaps again RAB-11) stimulates EXC-5. Further research on the function of various Rab proteins and guanine exchange factors at the canal apical surface should provide a fruitful avenue of study.

Implications: Modeling tubule growth

Several alternative hypotheses can explain how these interactions form the terminal web and guide outgrowth of the canal lumen. One attractive hypothetical model is shown in Fig. 8. EXC-1/IRG is associated with the membrane along the entire length of the canal. At sites where EXC-1 is exposed to the cytoplasm (i.e., at the growing canal tip and at sites of membrane

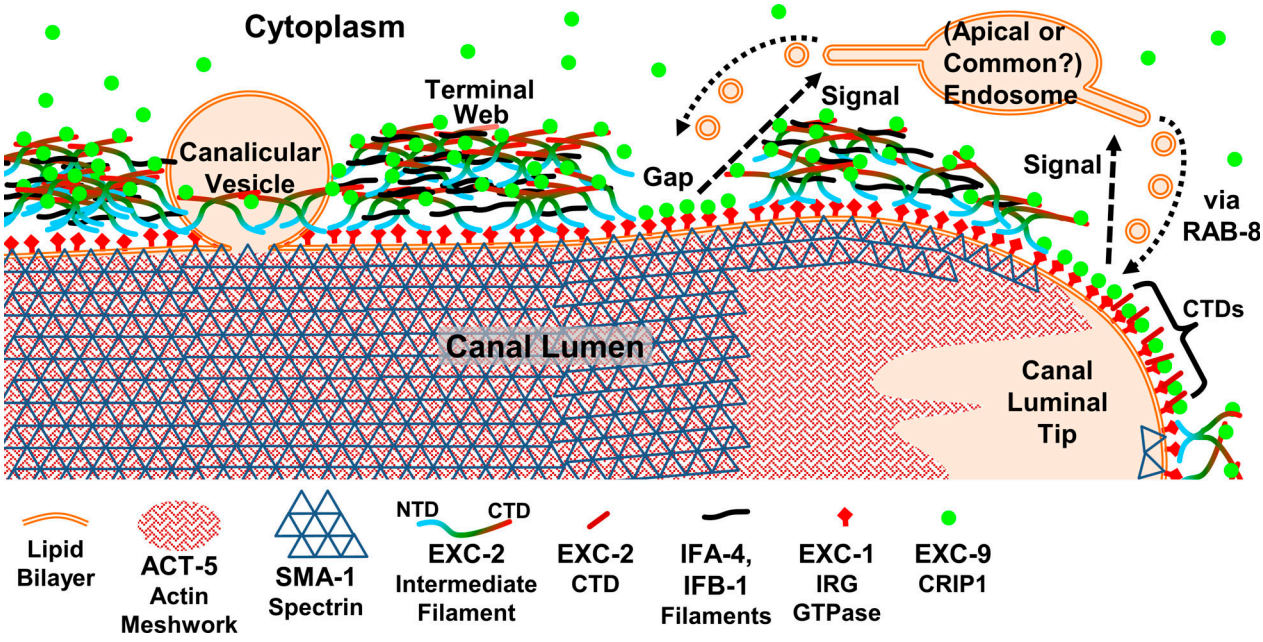

Figure 8. **Hypothetical model of extension of the excretory canal lumen.** Diagram of distal end of a canal showing the canal lumen and terminal web within the cytoplasm. Most proteins are shown in a narrow plane of focus, but ACT-5 actin and SMA-1 spectrin are shown covering the luminal membrane on all sides; these are presumed to be added as the canal grows during development (right-hand side of the diagram). EXC-1/IRG is linked to the luminal membrane (via presumed myristoylation site), while most EXC-9 is retained by the C-terminus of the EXC-2 component of the terminal web. In regions of osmotic stress ("Gap") or rapid growth (right-hand end), the terminal web is thinned or missing, and EXC-9 can make contact with and activate EXC-1. EXC-1 then directly or indirectly (thick dashed arrows) stimulates RAB-8 to deliver vesicles (thin dashed arrows), containing cargo of unknown identity, that help rebuild or strengthen the cytoskeleton at that location. Overexpressed EXC-2 CTD (short red lines on right) blocks EXC-1 activity.

addition during growth, such as evenly spaced "beads" in the L1 stage; Kolotuev et al., 2013), soluble EXC-9/CRIP can bind to and activate EXC-1 (Grussendorf et al., 2016), as well as be retained by the CTD of EXC-2. EXC-1 then directs the movement of vesicles via RAB-8 and/or via guanine exchange factor EXC-5/FGD to facilitate actin polymerization for vesicle delivery to that area of the tubules. Polymerization of cytoskeletal elements ACT-5/actin, SMA-1/spectrin, and the three intermediate filaments EXC-2, IFA-4, and IFB-1 follows.

While the present results provide a plausible framework by which intermediate filaments can serve as a luminal scaffold for proteins that regulate directed tubular growth, other models are equally plausible. Future studies examining the biochemistry of EXC-1 and EXC-9 activation during canal development will be invaluable in understanding tubular growth mediated by these two proteins and by intermediate filaments. Recent manuscripts on bioRxiv (Sun et al., 2020 *Preprint*; Winkelman et al., 2020 *Preprint*; not yet peer reviewed) suggest that other LIM-domain proteins are capable of measuring tension in cytoskeletal actin filaments. The growing excretory canal could provide an example of where the LIM domain of CRIP is performing a similar function with the stretchable domains of intermediate filaments. This model of the excretory canal potentially suggests that cytoskeletal filaments as measured by CRIP/LIM–domain proteins for repair/growth via IRG proteins and vesicle transport could be a widespread mechanism for growth and repair of cytoskeletal elements linked to membrane. The homology of EXC-9 to CRIP and EXC-1 to the IRG family of proteins (including the autophagy regulator IRGM) suggests that study of the excretory canal cell provides a model for greater understanding of the regulation of these ubiquitous mammalian proteins.

Materials and methods

C. elegans strains

C. elegans strains were grown on BK16 bacteria (a streptomycin-resistant derivative of OP50; Brenner, 1974) at 20C according to standard techniques. All strains used are listed in Table S1.

DNA constructs and plasmids

EXC-2 NTD (amino acids 1–767), EXC-2 CTD (amino acids 1112–1339), RAB-8, and GFP::RAB-11.1 constructs were built by means of Gibson assembly (NEBuilder HiFi DNA Assembly Master Mix, Cat. #E2621S). pCV01 (Oka and Futai, 2000) was used as the backbone vector. Detailed primers are listed in Table S2. CRISPR/Cas9 modifications were performed according to the protocols of the Goldstein laboratory (Dickinson et al., 2015). The sites of modifications made are shown in Table S3.

Microscopy

Animals were examined via a Zeiss Axioskop microscope equipped for both epifluorescence and differential interference contrast microscopy with 40× (NA 1.3) and 63× (NA 1.4) objectives, and photographs were captured by use of an Optronics MagnaFire Camera. Animals were placed on 2% agarose pads in M9 solution + 35 mM NaN_3. Contrast on DIC images was

uniformly enhanced over the entire image to increase clarity. The subcellular location of fluorescent proteins at high resolution was examined through a FluoView FV1000 laser-scanning confocal microscope (Olympus) with 60× objective (NA 1.42). Lasers were set to 488-nm excitation and 520-nm emission (for GFP and CFP) or 543-nm excitation and 572-nm emission (for mKate2 and mCherry). All confocal images were captured via FluoView software (Olympus), and collocation was analyzed by use of ImageJ software. Fluorescent images from both microscopes were false-colored (green to cyan, red to magenta). Electron microscopy on thin sections of immersion-fixed animals was performed on a Philips CM10 electron microscope following standard methods (Hall, 1995).

Statistical analysis

Canal length was measured as a percentage of full-length posterior canals (reaching past the anus); full length was rated 100%; canals reaching to the vulva in the center of the animal, 50%; and complete lack of extension, 0%; lengths between these landmarks were interpolated. Comparisons of canal length and of percentage of convoluted canals were calculated via one-way ANOVA.

Brightness of expression in the canals was measured in ImageJ by measuring brightness along a line perpendicular to the animal of maximum width (300 pixels). Average brightness of the background was subtracted from all, then the ratio of average brightness in areas outside of the canal was subtracted from average brightness in the area of the canal. The ratio of canal-specific brightness to brightness of the worm overall was plotted (e.g., Fig. 7 C).

Online supplemental material

Fig. S1 shows the expression pattern of EXC-9 outside the excretory canals. Fig. S2 shows the expression pattern of EXC-1 outside the excretory canals. Table S1 lists the strains used for this study. Table S2 lists the primers used for making constructs. Table S3 lists the mutations induced via CRISPR/Cas9 injection.

Acknowledgments

We thank anonymous reviewers for substantial improvements to the manuscript and for pointing out the recent studies of LIM-domain proteins on bioRxiv.org.

Z. Yang was supported by Kansas University Graduate Research fund no. 2144091. D.H. Hall was supported by National Institutes of Health OD 010943. Some strains were provided by the *Caenorhabditis* Genetics Center, which is funded by the National Institutes of Health, Office of Research Infrastructure Programs (P40 OD-010440).

The authors declare no competing financial interests.

Author contributions: Z. Yang participated in conceptualization; carried out the investigation, visualization, and use of software; and wrote the original draft. B.C. Mattingly participated in the investigation to create strains. D.H. Hall participated in investigation and visualization and analysis of electron micrographs. B.D. Ackley provided resources and methodology for acquisition of confocal images. M. Buechner was responsible for overall conceptualization, supervision, resources, and visualization and reviewed and edited the manuscript.

Submitted: 25 March 2020
Revised: 15 June 2020
Accepted: 3 August 2020

References

Al-Hashimi, H., D.H. Hall, B.D. Ackley, E.A. Lundquist, and M. Buechner. 2018. Tubular Excretory Canal Structure Depends on Intermediate Filaments EXC-2 and IFA-4 in *Caenorhabditis elegans*. *Genetics*. 210: 637–652.

Al-Hashimi, H., T. Chiarelli, E.A. Lundquist, and M. Buechner. 2019. Novel *exc* Genes Involved in Formation of the Tubular Excretory Canals of *Caenorhabditis elegans*. *G3 (Bethesda)*. 9:1339–1353. https://doi.org/10.1534/g3.119.200626

Ang, A.L., H. Fölsch, U.-M. Koivisto, M. Pypaert, and I. Mellman. 2003. The Rab8 GTPase selectively regulates AP-1B-dependent basolateral transport in polarized Madin-Darby canine kidney cells. *J. Cell Biol.* 163: 339–350. https://doi.org/10.1083/jcb.200307046

Armenti, S.T., E. Chan, and J. Nance. 2014. Polarized exocyst-mediated vesicle fusion directs intracellular lumenogenesis within the C. elegans excretory cell. *Dev. Biol.* 394:110–121. https://doi.org/10.1016/j.ydbio.2014.07.019

Barry, D.M., K. Xu, S.M. Meadows, Y. Zheng, P.R. Norden, G.E. Davis, and O. Cleaver. 2015. Cdc42 is required for cytoskeletal support of endothelial cell adhesion during blood vessel formation in mice. *Development*. 142: 3058–3070. https://doi.org/10.1242/dev.125260

Bellec, K., I. Gicquel, and R. Le Borgne. 2018. Stratum recruits Rab8 at Golgi exit sites to regulate the basolateral sorting of Notch and Sanpodo. *Development*. 145. dev163469. https://doi.org/10.1242/dev.163469

Berry, K.L., H.E. Bulow, D.H. Hall, and O. Hobert. 2003. A C. elegans CLIC-like protein required for intracellular tube formation and maintenance. *Science*. 302:2134–2137.

Brenner, S.. 1974. The genetics of *Caenorhabditis elegans*. *Genetics*. 77:71–94.

Buechner, M., D.H. Hall, H. Bhatt, and E.M. Hedgecock. 1999. Cystic canal mutants in *Caenorhabditis elegans* are defective in the apical membrane domain of the renal (excretory) cell. *Dev. Biol.* 214:227–241. https://doi.org/10.1006/dbio.1999.9398

Carberry, K., T. Wiesenfahrt, R. Windoffer, O. Bossinger, and R.E. Leube. 2009. Intermediate filaments in Caenorhabditis elegans. *Cell Motil. Cytoskeleton*. 66:852–864. https://doi.org/10.1002/cm.20372

Chiou, J.G., M.K. Balasubramanian, and D.J. Lew. 2017. Cell Polarity in Yeast. *Annu. Rev. Cell Dev. Biol.* 33:77–101. https://doi.org/10.1146/annurev-cellbio-100616-060856

Coch, R.A., and R.E. Leube. 2016. Intermediate Filaments and Polarization in the Intestinal Epithelium. *Cells*. 5:32. https://doi.org/10.3390/cells5030032

Cousins, R.J., and L. Lanningham-Foster. 2000. Regulation of cysteine-rich intestinal protein, a zinc finger protein, by mediators of the immune response. *J. Infect. Dis.* 182(Suppl 1):S81–S84. https://doi.org/10.1086/315917

Davis, B.A., R.K. Blanchard, L. Lanningham-Foster, and R.J. Cousins. 1998. Structural characterization of the rat cysteine-rich intestinal protein gene and overexpression of this LIM-only protein in transgenic mice. *DNA Cell Biol.* 17:1057–1064. https://doi.org/10.1089/dna.1998.17.1057

Delacour, D., J. Salomon, S. Robine, and D. Louvard. 2016. Plasticity of the brush border - the yin and yang of intestinal homeostasis. *Nat. Rev. Gastroenterol. Hepatol.* 13:161–174. https://doi.org/10.1038/nrgastro.2016.5

Delague, V., A. Jacquier, T. Hamadouche, Y. Poitelon, C. Baudot, I. Boccaccio, E. Chouery, M. Chaouch, N. Kassouri, R. Jabbour, et al. 2007. Mutations in FGD4 encoding the Rho GDP/GTP exchange factor FRABIN cause autosomal recessive Charcot-Marie-Tooth type 4H. *Am. J. Hum. Genet.* 81:1–16. https://doi.org/10.1086/518428

Dickinson, D.J., A.M. Pani, J.K. Heppert, C.D. Higgins, and B. Goldstein. 2015. Streamlined Genome Engineering with a Self-Excising Drug Selection Cassette. *Genetics*. 200:1035–1049. https://doi.org/10.1534/genetics.115.178335

Dodemont, H., D. Riemer, N. Ledger, and K. Weber. 1994. Eight genes and alternative RNA processing pathways generate an unexpectedly large

diversity of cytoplasmic intermediate filament proteins in the nematode Caenorhabditis elegans. *EMBO J.* 13:2625–2638. https://doi.org/10.1002/j.1460-2075.1994.tb06553.x

Falin, R.A., R. Morrison, A.J. Ham, and K. Strange. 2009. Identification of regulatory phosphorylation sites in a cell volume- and Ste20 kinase-dependent ClC anion channel. *J. Gen. Physiol.* 133:29–42. https://doi.org/10.1085/jgp.200810080

Flibotte, S., M.L. Edgley, I. Chaudhry, J. Taylor, S.E. Neil, A. Rogula, R. Zapf, M. Hirst, Y. Butterfield, S.J. Jones, et al. 2010. Whole-genome profiling of mutagenesis in Caenorhabditis elegans. *Genetics.* 185:431–441. https://doi.org/10.1534/genetics.110.116616

Fujita, M., D. Hawkinson, K.V. King, D.H. Hall, H. Sakamoto, and M. Buechner. 2003. The role of the ELAV homologue EXC-7 in the development of the Caenorhabditis elegans excretory canals. *Dev. Biol.* 256: 290–301. https://doi.org/10.1016/S0012-1606(03)00040-X

Gao, J., L. Estrada, S. Cho, R.E. Ellis, and J.L. Gorski. 2001. The Caenorhabditis elegans homolog of FGD1, the human Cdc42 GEF gene responsible for faciogenital dysplasia, is critical for excretory cell morphogenesis. *Hum. Mol. Genet.* 10:3049–3062. https://doi.org/10.1093/hmg/10.26.3049

Geisler, F., R.A. Coch, C. Richardson, M. Goldberg, C. Bevilacqua, R. Prevedel, and R.E. Leube. 2020. Intestinal intermediate filament polypeptides in C. elegans: Common and isotype-specific contributions to intestinal ultrastructure and function. *Sci. Rep.* 10:3142. https://doi.org/10.1038/s41598-020-59791-w

Gerace, L., and B. Burke. 1988. Functional organization of the nuclear envelope. *Annu. Rev. Cell Biol.* 4:335–374. https://doi.org/10.1146/annurev.cb.04.110188.002003

Gruenbaum, Y., and R. Foisner. 2015. Lamins: nuclear intermediate filament proteins with fundamental functions in nuclear mechanics and genome regulation. *Annu. Rev. Biochem.* 84:131–164. https://doi.org/10.1146/annurev-biochem-060614-034115

Grussendorf, K.A., C.J. Trezza, A.T. Salem, H. Al-Hashimi, B.C. Mattingly, D.E. Kampmeyer, L.A. Khan, D.H. Hall, V. Göbel, B.D. Ackley, et al. 2016. Facilitation of Endosomal Recycling by an IRG Protein Homolog Maintains Apical Tubule Structure in Caenorhabditis elegans. *Genetics.* 203:1789–1806. https://doi.org/10.1534/genetics.116.192559

Hakanen, J., N. Ruiz-Reig, and F. Tissir. 2019. Linking Cell Polarity to Cortical Development and Malformations. *Front. Cell. Neurosci.* 13:244. https://doi.org/10.3389/fncel.2019.00244

Hall, D.H.. 1995. Electron Microscopy and Three-Dimensional Image Reconstruction. *In* Caenorhabditis Elegans: Modern Biological Analysis of an Organism. Vol. Vol. 48. H.F. Epstein, and D.C. Shakes, editors. Academic Press, San Diego. pp. 451–482.

He, G., L. Zou, L. Zhou, P. Gao, X. Qian, and J. Cui. 2017. Cysteine-Rich Intestinal Protein 1 Silencing Inhibits Migration and Invasion in Human Colorectal Cancer. *Cell. Physiol. Biochem.* 44:897–906. https://doi.org/10.1159/000485357

Herrmann, H., and U. Aebi. 2016. Intermediate Filaments: Structure and Assembly. *Cold Spring Harb. Perspect. Biol.* 8. a018242. https://doi.org/10.1101/cshperspect.a018242

Howard, J.C., J.P. Hunn, and T. Steinfeldt. 2011. The IRG protein-based resistance mechanism in mice and its relation to virulence in Toxoplasma gondii. *Curr. Opin. Microbiol.* 14:414–421. https://doi.org/10.1016/j.mib.2011.07.002

Hüsken, K., T. Wiesenfahrt, C. Abraham, R. Windoffer, O. Bossinger, and R.E. Leube. 2008. Maintenance of the intestinal tube in Caenorhabditis elegans: the role of the intermediate filament protein IFC-2. *Differentiation.* 76:881-s3. https://doi.org/10.1111/j.1432-0436.2008.00264.x

Igual Gil, C., M. Jarius, J.P. von Kries, and A.K. Rohlfing. 2017. Neuronal Chemosensation and Osmotic Stress Response Converge in the Regulation of *aqp-8* in *C. elegans*. *Front. Physiol.* 8:380. https://doi.org/10.3389/fphys.2017.00380

Johnson, D.R., R.S. Bhatnagar, L.J. Knoll, and J.I. Gordon. 1994. Genetic and biochemical studies of protein N-myristoylation. *Annu. Rev. Biochem.* 63: 869–914. https://doi.org/10.1146/annurev.bi.63.070194.004253

Karabinos, A.. 2019. Intermediate filament (IF) proteins IFA-1 and IFB-1 represent a basic heteropolymeric IF cytoskeleton of nematodes: A molecular phylogeny of nematode IFs. *Gene.* 692:44–53. https://doi.org/10.1016/j.gene.2018.12.069

Karabinos, A., H. Schmidt, J. Harborth, R. Schnabel, and K. Weber. 2001. Essential roles for four cytoplasmic intermediate filament proteins in Caenorhabditis elegans development. *Proc. Natl. Acad. Sci. USA.* 98: 7863–7868. https://doi.org/10.1073/pnas.121169998

Karabinos, A., J. Schünemann, and D.A. Parry. 2017. Assembly studies of six intestinal intermediate filament (IF) proteins B2, C1, C2, D1, D2, and E1 in the nematode C. elegans. *Cytoskeleton (Hoboken).* 74:107–113. https://doi.org/10.1002/cm.21354

Khan, L.A., H. Zhang, N. Abraham, L. Sun, J.T. Fleming, M. Buechner, D.H. Hall, and V. Gobel. 2013. Intracellular lumen extension requires ERM-1-dependent apical membrane expansion and AQP-8-mediated flux. *Nat. Cell Biol.* 15:143–156. https://doi.org/10.1038/ncb2656

Khan, L.A., G. Jafari, N. Zhang, E. Membreno, S. Yan, H. Zhang, and V. Gobel. 2019. A tensile trilayered cytoskeletal endotube drives capillary-like lumenogenesis. *J. Cell Biol.* 218:2403–2424. https://doi.org/10.1083/jcb.201811175

Kiral, F.R., F.E. Kohrs, E.J. Jin, and P.R. Hiesinger. 2018. Rab GTPases and Membrane Trafficking in Neurodegeneration. *Curr. Biol.* 28:R471–R486. https://doi.org/10.1016/j.cub.2018.02.010

Kolotuev, I., V. Hyenne, Y. Schwab, D. Rodriguez, and M. Labouesse. 2013. A pathway for unicellular tube extension depending on the lymphatic vessel determinant Prox1 and on osmoregulation. *Nat. Cell Biol.* 15: 157–168. https://doi.org/10.1038/ncb2662

Kumar, S., A. Jain, F. Farzam, J. Jia, Y. Gu, S.W. Choi, M.H. Mudd, A. Claude-Taupin, M.J. Wester, K.A. Lidke, et al. 2018. Mechanism of Stx17 recruitment to autophagosomes via IRGM and mammalian Atg8 proteins. *J. Cell Biol.* 217:997–1013. https://doi.org/10.1083/jcb.201708039

Lant, B., B. Yu, M. Goudreault, D. Holmyard, J.D. Knight, P. Xu, L. Zhao, K. Chin, E. Wallace, M. Zhen, et al. 2015. CCM-3/STRIPAK promotes seamless tube extension through endocytic recycling. *Nat. Commun.* 6: 6449. https://doi.org/10.1038/ncomms7449

Li, H.G., L.H. Zhao, Z.H. Zhang, J.Z. Liu, K. Ren, S.Y. Li, and Z.J. Su. 2017. The Impact of Cysteine-Rich Intestinal Protein 1 (CRIP1) on Thyroid Carcinoma. *Cell. Physiol. Biochem.* 43:2037–2046. https://doi.org/10.1159/000484184

Mack, N.A., and M. Georgiou. 2014. The interdependence of the Rho GTPases and apicobasal cell polarity. *Small GTPases.* 5. e973768. https://doi.org/10.4161/21541248.2014.973768

Mattingly, B.C., and M. Buechner. 2011. The FGD homologue EXC-5 regulates apical trafficking in C. elegans tubules. *Dev. Biol.* 359:59–72. https://doi.org/10.1016/j.ydbio.2011.08.011

Neefjes, J., and R. van der Kant. 2014. Stuck in traffic: an emerging theme in diseases of the nervous system. *Trends Neurosci.* 37:66–76. https://doi.org/10.1016/j.tins.2013.11.006

Nelson, F.K., P.S. Albert, and D.L. Riddle. 1983. Fine structure of the *Caenorhabditis elegans* secretory-excretory system. *J. Ultrastruct. Res.* 82: 156–171. https://doi.org/10.1016/S0022-5320(83)90050-3

Nemetschke, L., and E. Knust. 2016. Drosophila Crumbs prevents ectopic Notch activation in developing wings by inhibiting ligand-independent endocytosis. *Development.* 143:4543–4553. https://doi.org/10.1242/dev.141762

Oka, T., and M. Futai. 2000. Requirement of V-ATPase for ovulation and embryogenesis in Caenorhabditis elegans. *J. Biol. Chem.* 275:29556–29561. https://doi.org/10.1074/jbc.M002756200

Pilla-Moffett, D., M.F. Barber, G.A. Taylor, and J. Coers. 2016. Interferon-inducible GTPases in host resistance, inflammation and disease. *J. Mol. Biol.* 428:3495–3513. https://doi.org/10.1016/j.jmb.2016.04.032

Pires, H.R., and M. Boxem. 2018. Mapping the Polarity Interactome. *J. Mol. Biol.* 430:3521–3544. https://doi.org/10.1016/j.jmb.2017.12.017

Praitis, V., E. Ciccone, and J. Austin. 2005. SMA-1 spectrin has essential roles in epithelial cell sheet morphogenesis in C. elegans. *Dev. Biol.* 283: 157–170. https://doi.org/10.1016/j.ydbio.2005.04.002

Román-Fernández, Á., J. Roignot, E. Sandilands, M. Nacke, M.A. Mansour, L. McGarry, E. Shanks, K.E. Mostov, and D.M. Bryant. 2018. The phospholipid PI(3,4)P_2 is an apical identity determinant. *Nat. Commun.* 9: 5041. https://doi.org/10.1038/s41467-018-07464-8

Sato, T., S. Mushiake, Y. Kato, K. Sato, M. Sato, N. Takeda, K. Ozono, K. Miki, Y. Kubo, A. Tsuji, et al. 2007. The Rab8 GTPase regulates apical protein localization in intestinal cells. *Nature.* 448:366–369. https://doi.org/10.1038/nature05929

Sato, K., A. Norris, M. Sato, and B.D. Grant. 2014. C. elegans as a model for membrane traffic. *WormBook.* 1–47. https://doi.org/10.1895/wormbook.1.77.2

Shaye, D.D., and I. Greenwald. 2015. The disease-associated formin INF2/EXC-6 organizes lumen and cell outgrowth during tubulogenesis by regulating F-actin and microtubule cytoskeletons. *Dev. Cell.* 32:743–755. https://doi.org/10.1016/j.devcel.2015.01.009

Sigurbjörnsdóttir, S., R. Mathew, and M. Leptin. 2014. Molecular mechanisms of de novo lumen formation. *Nat. Rev. Mol. Cell Biol.* 15:665–676. https://doi.org/10.1038/nrm3871

Smith, M.A., E. Blankman, M.L. Gardel, L. Luettjohann, C.M. Waterman, and M.C. Beckerle. 2010. A zyxin-mediated mechanism for actin stress fiber

maintenance and repair. *Dev. Cell*. 19:365–376. https://doi.org/10.1016/j.devcel.2010.08.008

Stendel, C., A. Roos, T. Deconinck, J. Pereira, F. Castagner, A. Niemann, J. Kirschner, R. Korinthenberg, U.P. Ketelsen, E. Battaloglu, et al. 2007. Peripheral nerve demyelination caused by a mutant Rho GTPase guanine nucleotide exchange factor, frabin/FGD4. *Am. J. Hum. Genet*. 81:158–164. https://doi.org/10.1086/518770

Sun, X., D.Y.Z. Phua, L. Axiotakis, M.A. Smith, E. Blankman, R. Gong, R.C. Cail, S. Espinosa de Los Reyes, M.C. Beckerle, C.M. Waterman, et al. 2020. Mechanosensing through direct binding of tensed F-actin by LIM domains. *bioRxiv*. doi:10.1101/2020.03.06.979245 (Preprint posted March 7, 2020).

Sundaram, M.V., and M. Buechner. 2016. The Caenorhabditis elegans Excretory System: A Model for Tubulogenesis, Cell Fate Specification, and Plasticity. *Genetics*. 203:35–63. https://doi.org/10.1534/genetics.116.189357

Sundaram, M.V., and J.D. Cohen. 2017. Time to make the doughnuts: Building and shaping seamless tubes. *Semin. Cell Dev. Biol*. 67:123–131. https://doi.org/10.1016/j.semcdb.2016.05.006

Tong, X., and M. Buechner. 2008. CRIP homologues maintain apical cytoskeleton to regulate tubule size in C. elegans. *Dev. Biol*. 317:225–233. https://doi.org/10.1016/j.ydbio.2008.02.040

Udenwobele, D.I., R.C. Su, S.V. Good, T.B. Ball, S. Varma Shrivastav, and A. Shrivastav. 2017. Myristoylation: An Important Protein Modification in the Immune Response. *Front. Immunol*. 8:751. https://doi.org/10.3389/fimmu.2017.00751

Weiskirchen, R., and K. Günther. 2003. The CRP/MLP/TLP family of LIM domain proteins: acting by connecting. *BioEssays*. 25:152–162. https://doi.org/10.1002/bies.10226

Winkelman, J.D., C.A. Anderson, C. Suarez, D.R. Kovar, and M.L. Gardel. 2020. Evolutionarily diverse LIM domain-containing proteins bind stressed actin filaments through a conserved mechanism. *bioRxiv*. doi:10.1101/2020.03.06.980649 (Preprint posted March 7, 2020).

Wirshing, A.C.E., and E.J. Cram. 2018. Spectrin regulates cell contractility through production and maintenance of actin bundles in the Caenorhabditis elegans spermatheca. *Mol. Biol. Cell*. 29:2433–2449. https://doi.org/10.1091/mbc.E18-06-0347

Xie, Y., Y. Zheng, H. Li, X. Luo, Z. He, S. Cao, Y. Shi, Q. Zhao, Y. Xue, Z. Zuo, et al. 2016. GPS-Lipid: a robust tool for the prediction of multiple lipid modification sites. *Sci. Rep*. 6:28249. https://doi.org/10.1038/srep28249

Zhang, X., and N. Gao. 2016. RAB and RHO GTPases regulate intestinal crypt cell homeostasis and enterocyte function. *Small GTPases*. 7:59–64. https://doi.org/10.1080/21541248.2016.1159274

Zhang, L.Z., L.Y. Huang, A.L. Huang, J.X. Liu, and F. Yang. 2018. CRIP1 promotes cell migration, invasion and epithelial-mesenchymal transition of cervical cancer by activating the Wnt/β-catenin signaling pathway. *Life Sci*. 207:420–427. https://doi.org/10.1016/j.lfs.2018.05.054

Zuela, N., and Y. Gruenbaum. 2016. Intermediate Filaments in Caenorhabditis elegans. *Methods Enzymol*. 568:661–679. https://doi.org/10.1016/bs.mie.2015.09.020

Supplemental material

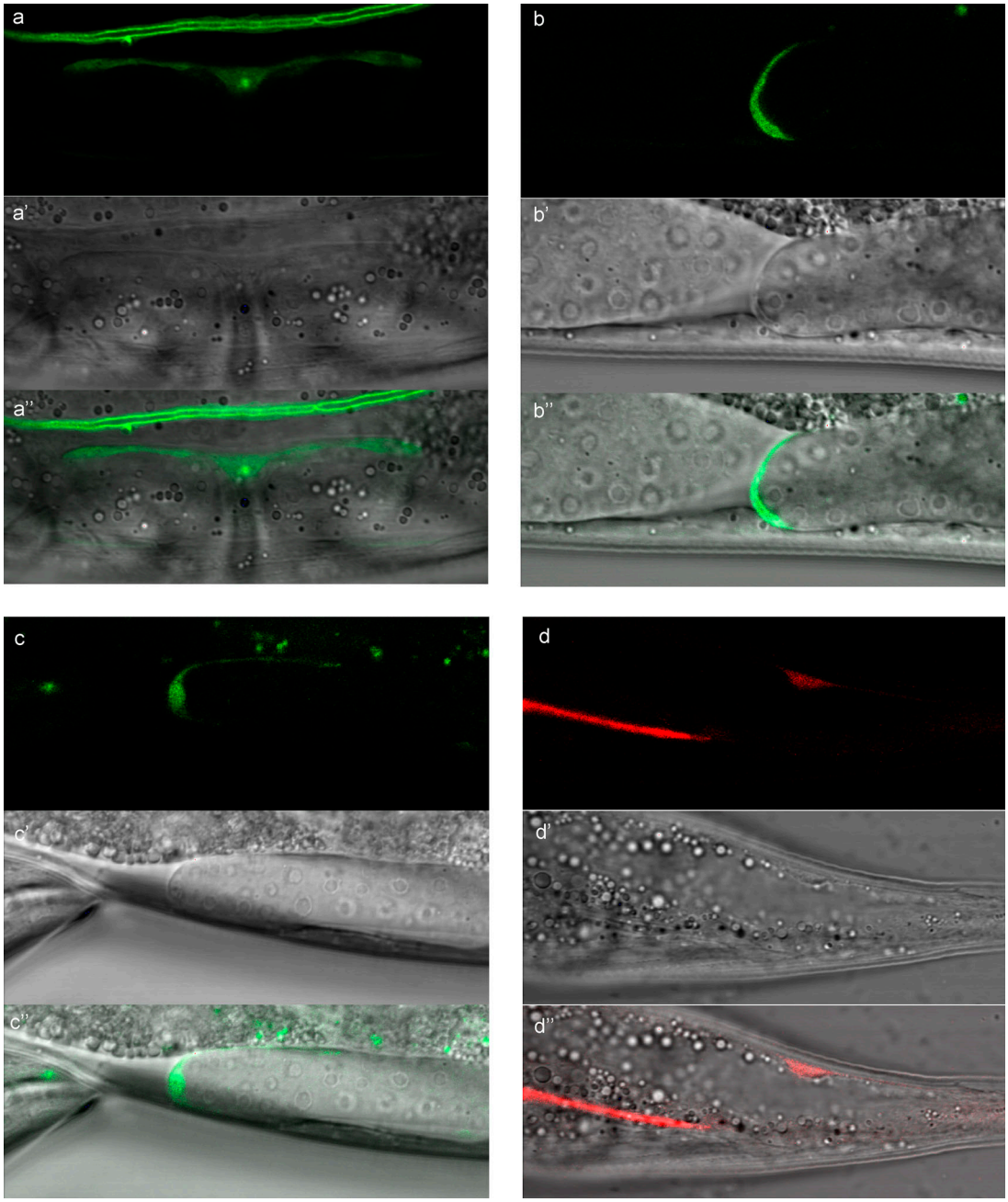

Figure S1. **EXC-9 expression pattern outside the excretory canals. (a–a'')**. EXC-9 shows expression in the uterine seam cell. **(b–d'')** Anterior and posterior gonadal distal tip cells (b–c'') within the lumbar ganglion (d–d''). For each set of micrographs, the top image shows fluorescence, the middle micrograph shows the DIC image, and bottom image is merged.

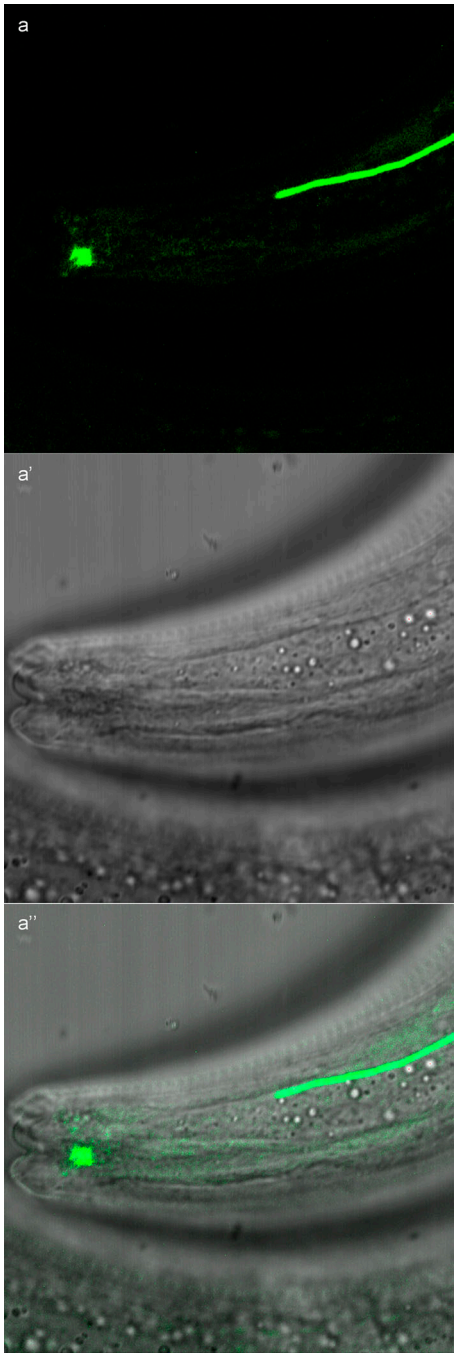

Figure S2. **EXC-1 expression pattern outside the excretory canals.** EXC-1 is strongly expressed within the tip of the amphid sheath cells. Fluorescent micrograph (a); DIC image (a'); and merge (a'').

Provided online are three tables. Table S1 lists the strains used for this study. Table S2 lists the primers used for making constructs. Table S3 lists the mutations induced via CRISPR/Cas9 injection.